SEPARATION SCIENCE AND TECHNOLOGY, 36(12), 2707–2731 (2001)

GLOBAL OPTIMIZATION OF REVERSE-FLOW GAS CYCLONES: APPLICATION TO SMALL-SCALE CYCLONE DESIGN

R. L. R. Salcedo* and M. G. Cândido

Departamento de Engenharia Química, Faculdade de Engenharia da Universidade do Porto, Rua Dr. Roberto Frias s/n, 4200-465 Porto

ABSTRACT

This paper addresses the optimum design of reverse-flow gas cyclones through the solution of 2 numerical nonlinear optimization problems that respectively maximize cyclone collection and an efficiency/cost ratio. The simulation model was based on the predictive properties of the 1998 finite diffusivity model of Mothes and Löffler, in which the particle turbulent dispersion coefficient is estimated through an empirical correlation between the radial Peclet and Reynolds numbers. The optimizations were formulated with constraints on pressure drop, saltation velocity, and geometrical considerations such that feasible cyclones could always be obtained. The two geometries, named RS_VHE and RS_K, are different from available high-efficiency designs and represent reverse-flow cyclones with a predicted, significantly improved performance. The geometry RS_VHE was built and tested on a laboratory scale, providing experimental evidence of a significantly improved design.

Key Words: Gas cyclones; Optimization; Turbulent dispersion

*Corresponding author. E-mail: rsalcedo@fe.up.pt

INTRODUCTION

Cyclones are gas-solid separation devices, characterized by low investment and operating costs, that can be used on heavily loaded gases or at high temperatures and pressures. The simulation of reverse-flow cyclones has been the subject of several different approaches (1–7). None of the proposed theories is capable of consistently giving good predictions when applied to experimental-grade collections obtained with different geometries, operating conditions, and particle-size distributions. Of all the theories, the Mothes and Löffler (5) and Iozia and Leith (7) models give the predictions that are best correlated with available data (7–11).

Computational fluid dynamics tools have also been successfully applied to the prediction of grade-efficiency curves in reverse-flow gas cyclones. Kessler and Leith (12) developed a numerical model based on measured turbulence flow fields in a cyclone, and with this model, they obtained a better agreement with the data of Dirgo and Leith (13) than was obtained by the Iozia and Leith (7) model. Hoffmann, de Groot, and Hospers (14), following the work of Boysan et al. (15), obtained a better agreement between theoretical predictions and experimental-grade efficiency curves with 4 reverse-flow cyclones than they did with the Mothes and Löffler (5) model. However, more basic research in turbulence is required before numerical modeling can be employed for an optimal design of gas cyclones. Another drawback of these models is that they are computationally intensive (12).

These difficulties have led designers to base cyclone geometries on empirical testing; as a result, most designers, following a widely accepted rule to successful cyclone design, only use geometries that have been experimentally tested (16). This tendency to design cyclones based on experimental results is confirmed by the large variety of different high-efficiency designs available in the literature (an even higher number of proprietary designs have not been made public). As an example, Ramachandran and Leith (17) gave a list of 98 different high-efficiency reverse-flow cyclone designs.

This paper addresses the problem of the optimum design of reverse-flow gas cyclones through numerical optimization techniques. The proposed method produces cyclone designs with a significantly improved predicted performance over other high-efficiency designs while obeying all imposed constraints. One of these designs was validated with laboratory-scale experiments that were performed under loading conditions clearly unfavorable for particulate collection.

THE SIMULATION MODEL

A reliable simulation model is required for the numerical optimization of reverse-flow gas cyclones. From the available collection models, we only discuss

those from Mothes and Löffler (5) and Iozia and Leith (7), because they have been shown to be, on the average, clearly superior to other cyclone collection models (7–11)

The Iozia and Leith (7) model relies on an empirical logistic function obtained by fitting collection data from 11 different cyclone geometries. By calculating performance indices (mean square deviations between observed and predicted efficiencies, mean differences, and corresponding variances for 216 grade-efficiency data points), Iozia and Leith showed that their model performs better than the models of Lapple (1), Barth (2), Leith and Licht (3), or Dietz (4). However, on average, it underpredicts collection (Fig. 8 in Iozia and Leith (7)).

The Mothes and Löffler (5) model extends the concept of Dietz (4) of particle interchange within different flow regions (entry region, down-flow annular region, and up-flow core region) by introducing a particle diffusivity (or turbulent dispersion) coefficient. This coefficient allows for particle concentrations to change continuously across the boundary between different regions, thus solving Dietz's discontinuity problem. The transport of particles in cyclones is then viewed as the superimposition of a diffusive motion (responsible mainly for the shape of the grade-efficiency curve) with a deterministic mean motion (which mainly defines the cyclone cut size). This model fits very well with available grade-efficiency data (10,11) if the particle dispersion coefficient is used as a fitting parameter. Predictions from the Mothes and Löffler (5) model are thus dependent on the knowledge of the particle turbulent-dispersion coefficient, which depends on operating conditions, cyclone geometry, and particle size (8). In 1999, Salcedo and Coelho (18) proposed that the particle turbulent dispersion coefficients can be estimated using an empirical correlation between the radial Peclet and Reynolds numbers:

$$\mathrm{Pe_p} = 0.0342\ \mathrm{Re_p^{1.263}} \tag{1}$$

where $\mathrm{Pe_p} = u_r d_p / D_r$ is the radial particle Peclet number; D_r is the radial dispersion coefficient; and $\mathrm{Re_p} = \rho d_p u_r / \mu$ is the radial particle Reynolds number. Statistical analysis showed the superiority of this correlation over other correlations proposed (6,19,20) or the use of a fixed value for the particle turbulent-dispersion coefficient (5,14).

Six small cyclones of 4 different geometries were built to test the applicability of the proposed relation, and using the Mothes and Löffler (5) theory, coupled with the proposed estimates of the turbulent dispersion coefficients, we predicted global and grade collections that were in reasonable agreement with the observed data. Also, on the average, the proposed model neither underpredicts nor overpredicts collection (Figs. 8c and 9 in Salcedo and Coelho (18)). However, more fundamental work must be done to arrive at more realistic estimates of the particle turbulent-dispersion coefficients under cyclone flow.

Table 1. Performance Indices from Iozia and Leith

Index	Iozia and Leith	Mothes and Löffler
$I = \sum \frac{(\eta_m - \eta_p)^2}{n}$	0.023	0.0166
$\Delta = \sum \frac{\eta_m - \eta_p}{n}$	0.037	$1.5 \times 10^{-16} \approx 0$
$s_\Delta^2 = \sum \frac{(\eta_m - \Delta)^2}{n - 1}$	0.022	0.0167

Iozia and Leith (7). Mothes and Löffler (5).

To compare both models, we computed the performance indices of Iozia and Leith (7) using the 162 grade-collection data points analyzed by Salcedo and Coelho (18). These performance indices are based on a least-squares mean deviation between predicted and measured collection efficiency (I), a mean deviation (Δ), and a variance estimate around this mean deviation s_Δ^2. Although the databases of the models are not identical, Table 1 shows that the Mothes and Löffler (5) model performs better than the Iozia and Leith model (7), with a mean difference close to zero and smaller variance, despite the smaller number of data points. Thus, in this paper we retained the Mothes and Löffler (5) model as the simulation model of cyclone performance in the optimization problems.

THE OPTIMIZATION PROBLEMS

Numerical Optimization

Because each cyclone manufacturer has its own design, the question of design superiority is relevant to our investigation. The scientific literature is scarce on the subject of cyclone optimization probably due to 2 factors: Until recently, no single theory could predict with a reasonable accuracy the behavior of an arbitrary-geometry cyclone under different operating conditions (5,7,8,18), and commercial spin-offs could be derived from innovative geometries (21). Also, the optimum design was unlikely to be found by empirical testing because too many design parameters are involved in a reverse-flow cyclone, which is essentially determined by 8 dimensions (Fig. 1).

Li, Zisheng, and Kuotsung (22), Schmidt (23), and Lidén and Gudmundsson (24) gave some clues on the design of optimized cyclones, but improvements remain essentially empirical. For example, Lidén and Gudmundsson (24) suggested that the steepness of the grade-efficiency curve may be independently

changed from the cyclone cut size by changing independently the vortex finder inner and outer diameters.

To our knowledge, only the works performed by Ramachandran and Leith (17) Dirgo and Leith (25) and Iozia and Leith (26) were directly related with cyclone-design optimization based on a cyclone simulation model. Dirgo and Leith (25) had used the Leith and Licht (3) collection model, coupled with the pressure-drop models of Stairmand and Barth (in 26), to predict cyclone performance. However, pilot-scale tests with the optimized geometries failed to produce any significant improvements. Ramachandran and Leith (17) and Iozia and Leith (26) used the logistic empirical collection efficiency model of Iozia and Leith (7), coupled with the pressure-drop models (26) or a new empirical model for pressure drop in reverse-flow gas cyclones (17,27), for simulation purposes. The new pressure-drop model was developed by empirically fitting pressure drop data for 98 cyclone designs, and based on performance indices, it compared favorably with other pressure drop models.

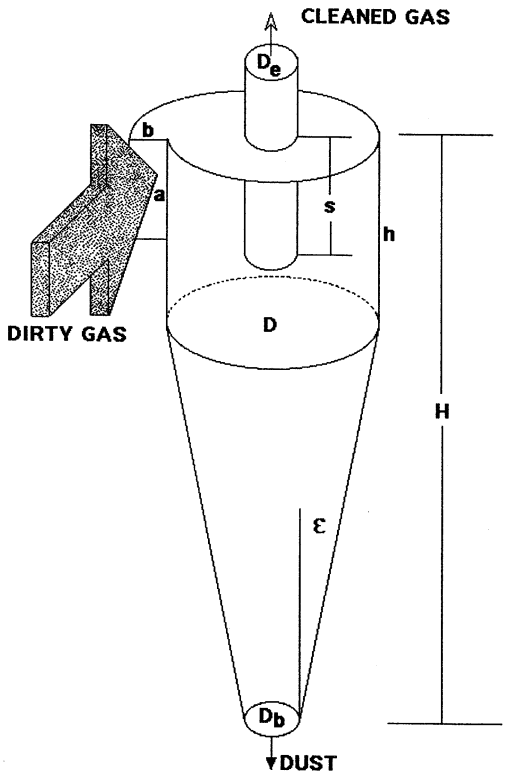

Figure 1. Typical reverse-flow cyclone.

These optimizations were carried out by a variation of the single factor method. A baseline design was set by fixing the cyclone diameter (D) at 0.254 m, the gas flow rate (Q) at 0.094 m^3/s, the outlet dust diameter (D_b) at 0.375 D, the cyclone cylinder height (h) at 1.5 D, the total height (H) at 5 D, and the pressure drop at a fixed value (varying from 0.1 to 4.0 kPa in steps of 0.1 kPa). The cyclone cut diameter (d_{50}) was computed for this baseline design using the Iozia and Leith model (7). Next, the vortex finder diameter D_e was varied as a primary variable, and pressure drop was reestablished (using a pressure-drop model) to the baseline value by adjusting inlet height (a), width (b), and vortex finder length (s) one at a time. The new cut diameter was next computed until it could not be further decreased outside of some small acceptable tolerance. After this preliminary optimization, the effect of changing cyclone height (between 4 D and 6 D) was studied. Thus, one may view this process as a suboptimization with 5 degrees of freedom (D_e, a, b, s, H). The result is that different optimized cyclone designs are obtained for each pressure drop model or within the same model because multiple solutions exist.

In this work, the optimum design of reverse-flow gas cyclones was based on a completely different approach. Because the Mothes and Löffler (5) model can be employed for predictive purposes with reasonable confidence (18), a full numerical optimization may be performed. Accordingly, we formulated 2 optimization problems: one for maximizing cyclone collection and one for optimizing the efficiency/cost ratio. The problems included several constraints on geometry, pressure drop, and saltation velocity, thus ensuring that feasible cyclones with efficiencies near the design efficiency were obtained. Saltation velocity is the tangential velocity near the cyclone wall that causes reentrainment of the collected particles. Because the tangential velocity is related to the cyclone inlet velocity and to the cyclone geometry, an upper limit of the cyclone inlet velocity exists above which the collection efficiency decreases due to reentrainment (28). The numerical optimization of a reverse-flow cyclone may thus be posed as the following problem:

Maximize any appropriate 'profit' function subject to

equality constraints:	*relevant design equations (cyclone modeling)*
	particle size distribution and particle density
	gas flow rate and dust load
	gas temperature, density and viscosity
inequality constraints:	*pressure loss*
	saltation velocity
	various geometric constraints

The profit function may be the overall collection efficiency or some cost-benefit criterion such as that proposed by Licht (28) for an efficiency/cost ratio. The equality constraints represent the problem data and the cyclone modeling theory. The inequality constraints represent bounds on the decision variables (the 8

cyclone dimensions) and on several dependent variables. Based on available literature, the following set of constraints was employed (17, 22,28–30):

$$\Delta P < \Delta P_{\max} \tag{2}$$

$$6.8^\circ < \varepsilon < 16^\circ \tag{3}$$

$$0.5 < \frac{4ab}{\pi D_e^2} < 0.735 \tag{4}$$

$$\frac{u_{in}}{u_s} < 1.25 \tag{5}$$

The first constraint (Eq. 2) limits the cyclone pressure drop because it is directly related to operating costs. In our work we have kept it limited to 1.5 kPa because this is a common value for high-efficiency cyclones. However, because of a large uncertainty on the estimation of this variable and because it may change drastically during the optimization process due to the changing geometries, we used 6 different methods to estimate ΔP; the methods were based on the models proposed by Barth (2), Bohnet and Lorenz (9), Dirgo (in 26), Stairmand (in 26), Shepherd and Lapple (31), and Caplan (32). The largest value obtained from the above models was retained for comparison with the imposed upper limit. This is a conservative option, and the optimum geometry might show lower pressure drops (as it eventually did).

The second constraint (Eq. 3) limits the cyclone cone semi-angle and reflects values that are associated with an easy dislodgement of the collected dust along the cyclone cone walls (28). The third constraint (Eq. 4) simply states that the effective cyclone gas discharge area should be larger than the entry section. The boundaries were found by inspecting sound cyclone designs (17,22,28). The last constraint (Eq. 5) puts an upper limit on the cyclone mean-entry velocity (u_{in}) but only in comparison with the saltation velocity (u_s), which is a function of cyclone geometry (varies during the optimization process), particle density, and operating conditions (28).

The geometric constraints were as follows (17,22,28,30):

$$s < h < H \tag{6}$$

$$0.5D_e < D_b < D_e \tag{7}$$

$$0.5(D - D_e) > b \tag{8}$$

$$s > 1.25a \tag{9}$$

$$2.3D_e \left(\frac{D^2}{ab}\right)^{\frac{1}{3}} < H - s \tag{10}$$

Equation (8) allows for an easy transition at the cyclone entry, while Eq. (9) allows for avoidance of short circuiting the gas. Equation 10 reflects the natural length of the cyclone (the length of the descending vortex below the vortex finder), as given by Alexander (33), which must not exceed the available cyclone height.

Due to the effect of the particle turbulent-dispersion coefficients, particle size distribution somewhat affects the optimized results. Therefore, the optimizations were performed with 2 very different distributions. Both corresponded to fine dusts with a lognormal distribution: a very fine $Ca(OH)_2$ dust with mean mass diameter (MMD) = 1.37 μm and $\sigma_g = 2.23$, such as used by Salcedo and Fonseca (11) and Campos (34), and a fine dust with MMD = 3.67 μm and $\sigma_g = 2.72$, such as used by Hoffmann et al. (14,21). The volumetric flow rate was set at 1, 10, 10^2, 10^3, and 10^4 Nm^3/h, with the lowest values representative of laboratory-scale cyclones and the highest representative of single industrial-scale cyclones.

The proposed problems are nonconvex, nonlinear, constrained optimization problems with 8 degrees of freedom. Because the diameter obeys the saltation and pressure drop constraints for a given set of operating conditions, it is not known beforehand and any arbitrary geometry that is chosen.

These problems were solved using a mixed integer nonlinear programming Salcedo-Gonçalves Azevedo algorithm, a robust, adaptive, random-search method (35,36). This algorithm probes the search space by randomly generating a biased sequence of preliminary solutions (cyclone designs), which are retained if all constraints are obeyed. The search space is decreased following the optimization sequence (history), eventually collapsing on a local optimum. Shifting strategies, which are temporary wrong-way movements (uphill for minimization or downhill for maximization), are included to allow the algorithm to escape local optima. For the general nonconvex, nonlinear programming problem, global optimum attainment is not guaranteed. However, the MSGA algorithm shows a great robustness for solving highly nonlinear nonconvex programming problems (37).

Optimized Geometries, Pressure Drop, and Predicted Performance

Optimized Geometries

The optimum geometry depends somewhat on flow rate and particle size distribution and is a highly undesirable variable for scale-up purposes. An effort was thus made to obtain 2 geometries, named RS_VHE and RS_K, that nearly maximize the global efficiency or the benefit/cost criterion of Licht (28). The patented intervals of cyclone ratios are given in Table 2 (38), where an optimized Iozia and Leith (26) design is also included for comparison. Due to commercial sensitivity, the exact geometries of the optimized cyclones cannot be disclosed, but the relative magnitudes of the dimensions that are thought to be most critical are as follows: geometries RS_VHE and RS_K both have essentially square entries; geometry RS_VHE has a cylindrical body about 50% shorter than a Stairmand HE design with an equivalent diameter, while geometry RS_K has a 50% longer body than a Stairmand HE design with an equivalent diameter; geometries RS_VHE and RS_K have both narrower vortex finders than a Stairmand HE

Table 2. Characteristic Dimensions of the Optimized Geometries

Ratio	RS_VHE	RS_K	Iozia and Leith
a/D	0.270–0.360	0.270–0.310	0.350
b/D	0.270–0.360	0.270–0.310	0.350
s/D	0.330–0.495	0.330–0.395	0.350
D_e/D	0.280–0.370	0.405–0.395	0.390
h/D	1.001–1.300	2.050–2.260	1.500
H/D	4.050–4.250	3.500–3.700	5.000
D_b/D	0.200–0.300	0.250–0.300	0.375

Iozia and Leith (7).

design with an equivalent diameter (design RS_VHE has the narrowest vortex finder). Design RS_VHE is about 6% longer than a Stairmand HE cyclone, while design RS_K is about 12% shorter than the Stairmand HE.

How different are the optimized cyclones from available designs? A literature survey was conducted on high-efficiency cyclone geometries, and 106 different designs were considered for comparison (17,22,26,28). The data presented in Fig. 2 allows one to see that the optimized geometries are significantly differ-

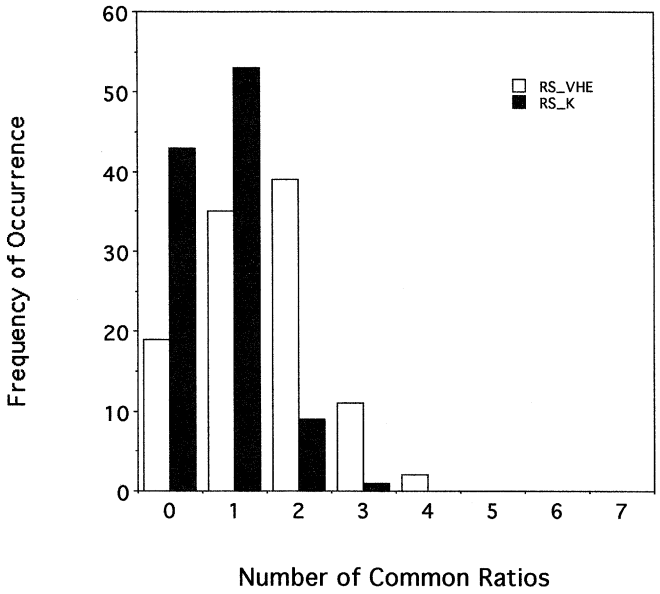

Figure 2. Histogram of common ratio occurrences with geometries RS_VHE and RS_K (Table 2) for 106 cyclone designs.

ent from available high-efficiency cyclones. In fact, for geometry RS_VHE only 2 designs that have 4 ratios are associated with the intervals given in Table 2, while design RS_K shares 3 common ratios (the Iozia and Leith optimized design in Table 2). Also, between 20 and 40 literature designs have nothing in common with the proposed designs.

Pressure Drop

The optimizations were performed with various pressure-drop models, and the maximum value was retained for comparison with the pressure-drop constraint because it was not known a priori which model should be chosen to predict this parameter for the optimized geometries. Thus, the pressure drop of the optimized geometries must eventually be measured. The measurement was performed for geometry RS_VHE (the highest efficiency geometry) on a laboratory-scale (D = 0.02 m) cyclone, at varying flow rates, using an online mass flowmeter and the method proposed by Ogawa (39) for pressure type cyclones. Figure 3 shows the average of 3 measurements $\pm$ 1 SD per design and shows that the Bohnet and Lorenz model (9) predicts results better than any other model.

The model of Dirgo (27) gives overpredictions very similar to those of the Barth (2) model. The number of velocity heads (ΔH) for the RS_VHE geometry

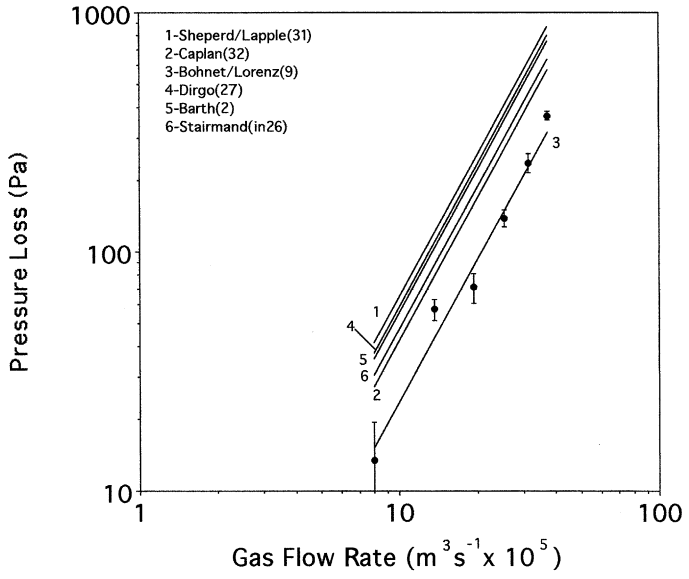

Figure 3. Pressure drop for the optimized RS_VHE design (D = 0.02 m).

computed through the pressure models of Dirgo (27) and Bohnet and Lorenz (9) was 9.4 and 3.4, respectively. In Fig. 2 of Ramachandran and Leith (17), ΔH is computed from the pressure-drop model of Dirgo (27) and compared with the measured value for 98 cyclone geometries. In the neighborhood of the computed value of 9.4, the data represented in this figure showed a large scatter in the observed number of velocity heads, varying from approximately 2 to 11. Thus, geometry RS_VHE has a much smaller number of velocity heads than estimated from Dirgo's model (27) but in the range of the experimental values reported by Ramachandran and Leith (17).

Predicted Performance

In a previous work (40), we compared the predicted performance for a suboptimal design (a locally optimum design) with that of several high-efficiency geometries, such as the Stairmand HE, Swift HE, Zhou #8 (an empirically optimized design), and a general purpose Peterson/Whitby design (22,28), in which we showed that the proposed geometry was always more efficient than those previously tested.

In this work, we compare the performance of the RS_VHE design with that of 2 high-efficiency geometries, such as the Stairmand HE and the optimized Iozia and Leith (7) geometry of Table 2. For purposes of illustration, we used the particle size distribution employed by Hoffmann et al. (14,21) and the cyclone baseline Stairmand HE design with $D = 0.254$ m at a flow rate of $Q = 0.094$ m^3/s. However, because different geometries may follow different pressure-drop models, we employed the pressure-drop model that best describes the behavior of the different geometries. For the Stairmand HE design, we used the Stairmand pressure-drop model (in 17); for the Iozia and Leith design (7), we used the Dirgo pressure-drop model (27); and for the RS_VHE design, we used the Bohnet and Lorenz (9) model.

Figure 4a shows a comparison between the predicted cyclone cut sizes against pressure drop; the superiority of the proposed RS_VHE design is clear. Figure 4b shows the scenario if all designs followed the pressure-loss model of Dirgo (27). Under the Dirgo model, the proposed design was the best when the pressure drop was 2 kPa or less, and the Iozia-Leith (7) design performed better at higher pressure losses. These figures show that the optimized design of reverse-flow gas cyclones is highly dependent on the pressure-drop model used, which is in agreement with the remarks of Iozia and Leith (26) and Ramachandran and Leith (17). Because the appropriate pressure-drop model is unknown during the optimization process, it must be experimentally determined for the optimized geometry. Thus, we expected that the predicted performance of the proposed RS_VHE geometry may be more realistically given by Fig. 4a rather than by Fig. 4b. However, due to the very small scale of the test cyclone, these results should

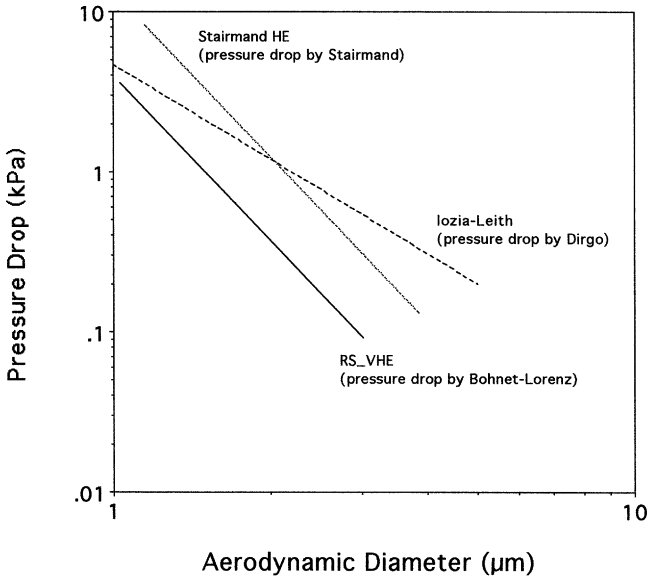

Figure 4a. Predicted pressure drop vs. d_{50} for 3 high-efficiency designs. $D = 0.254$ m; $Q = 0.094$ m^3/s; pressure drop models vary by design.

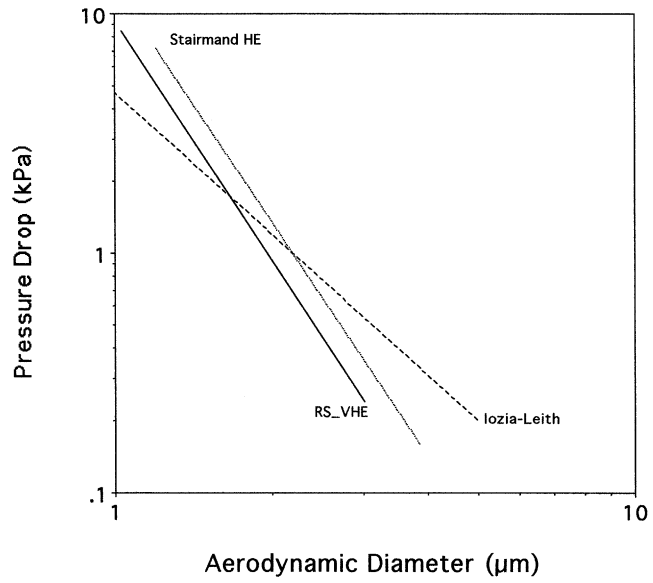

Figure 4b. Predicted pressure drop vs. d_{50} for 3 high-efficiency designs. $D = 0.254$ m; $Q = 0.094$ m^3/s; Dirgo (27) pressure drop model.

be taken with caution; no evidence exists to show that larger RS_VHE cyclones will follow the Bohnet and Lorenz (9) pressure-drop model.

EXPERIMENTAL VALIDATION

Size Distributions

To validate the proposed numerical optimization approach, one small laboratory-scale ($D = 0.02$m) RS_VHE cyclone was built. A similarly sized modified Stairmand HE design was also available for comparison. Dust concentrations of fine $Ca(OH)_2$ were always kept below 1.13×10^{-3} kg/m^3. Thus, dust loadings were small.

The dust was fed with a Wright Mk2 feeder, an improved electronically controlled version of the original all-mechanical Wright dust-feeding mechanism (41). Because this dust contains an appreciable fraction of submicron particles (approximately 3.6%) and a large proportion below 5 μm (approximately 63.4%), agglomeration is inevitable. To minimize the number of agglomerates fed to the test cyclone, a modified 0.07-m diameter Stairmand HE cyclone (10,11) was placed upstream of the test cyclone. Figure 5 shows a comparison of the particle

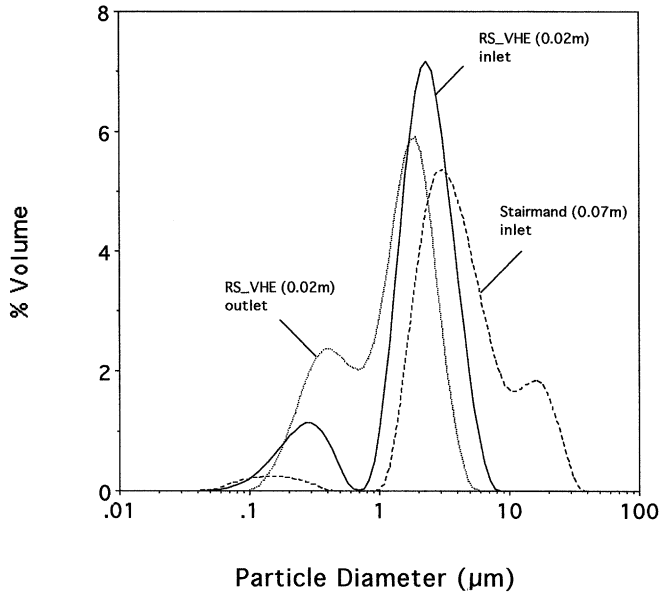

Figure 5. Particle size distributions before deagglomerating Stairmand HE cyclone and at inlet and exit of RS_VHE test cyclone (Coulter LS 230).

size distributions obtained upstream of the Stairmand HE cyclone and upstream and downstream of the test cyclone. The samples were collected on previously desiccated 47-mm GFA filters, dispersed in ethanol with ultrasound, and measured on a Coulter LS 230 laser particle sizer. The laser sizer has PIDS (polarization intensity differential scattering) capability for measuring submicron particles. The optical module illuminates the particles sequentially with vertically and horizontally polarized light of 3 different wavelengths. For each of the 3 wavelengths, the PIDS pattern, which is the difference in scattering between the 2 polarizations, is measured at several detectors centered approximately 90° from the incidence radiation (42).

Two filters were used in series to avoid a small amount of dust penetration from the first filter. Figure 5 clearly shows that the particle size distribution is shifted toward finer particles as the dust goes from the larger Stairmand HE inlet (median size 3.88 μm) to the RS_VHE inlet (median size 2.13 μm) and outlet (median size 1.35 μm), that the feed to the test cyclone is bimodal, and that particles above 8 μm have been removed by the deagglomerating cyclone. However, these distributions were obtained in a liquid medium under ultrasonic dispersion, and they may not reflect the actual distribution that enters the test cyclone.

Previous measurements on a similar sample captured at the inlet of the test cyclone by X-ray sedimentometry (11,18) with a Micromeritics 5100-D Sedigraph did not show a bimodal distribution but rather showed a lognormal distribution with MMD = 1.37 μm and $\sigma_g = 2.23$. This distribution was also obtained after particle redispersion in ethanol through ultrasound, but due to Brownian motion, the data for particles smaller than 1 μm should be considered with caution. The problem of small-particle measurements is not present in the Coulter LS 230 sizer, which can measure particles down to 0.04 μm due to PIDS capability. Figure 6a shows a comparison among the cumulative distributions obtained by both the X-ray 5100-D Sedigraph and the Coulter LS230 laser sizer. The differences are not surprising because these techniques measure different particle sizes: the X-ray Sedigraph measures the Stokesian diameter, which is the most appropriate diameter to characterize cyclone behavior; the Coulter measures an equivalent volume diameter. The values for these 2 different diameter measurements are only coincidental for spheres (43).

Scanning electron microscopy of the feed to the deagglomerating Stairmand 0.07-m cyclone (44) revealed that the individualized nonporous particles have a diameter between 0.05 and 1 μm, with an estimated mean diameter (from Brunauer-Emmett-Teller analysis) of 0.3 μm. These values are consistent with a MMD of approximately 2 μm (45); Fig. 6 shows a comparison between the Sedigraph (44) and the Coulter data. The better fit of the Sedigraph data could be due to nonspherical particles, which may cause problems with laser diffraction techniques (46).

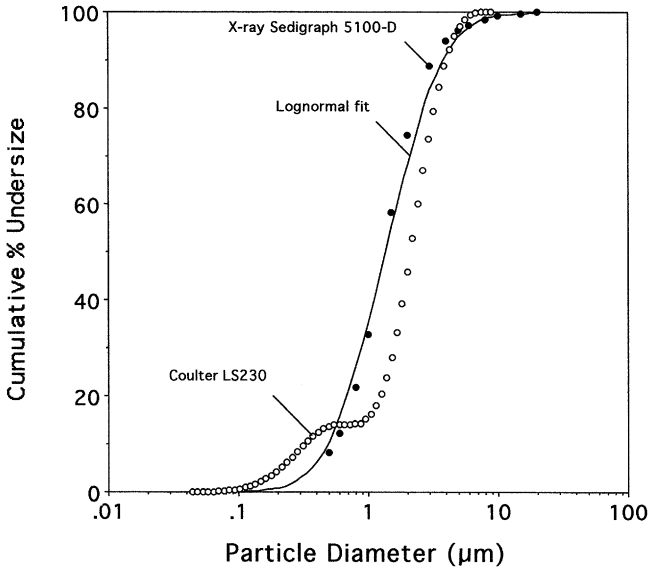

Figure 6. Particle size distributions at inlet of RS_VHE test cyclone obtained by different methods.

Global Collection

Global collection is not a good measurement of cyclone performance, particularly when different designs are compared, because pressure drop can vary widely. The global collection was first established by gravimetrical measurements of the dust entering and exiting the test cyclone at a flow rate of 2.52×10^{-4} m^3/s through 2 GFA 0.047-m filters in series. To avoid sampling losses during handling, the entire plastic lightweight filter holders were previously desiccated before weighing. Three runs were performed with the RS_VHE cyclone design for a minimum of 30 minutes to dampen fluctuations from the powder feeder, and a single run was made with the Stairmand HE design. The global collection was (average $\pm$ 1 SD) 78.3 $\pm$ 4.2% for the RS_VHE design. The similar-sized Stairmand HE design showed a lower collection efficiency of 57% and a somewhat lower pressure drop than did the RS_VHE. No further experiments were conducted with this design because previous results had shown the superiority of the numerically optimized designs at comparable pressure drops (34).

Table 3 shows a comparison between experimental collections with the global efficiencies predicted from the Mothes and Löffler (5) model. The data are based on the particle size distributions illustrated in Fig. 6. The predicted intervals are the expected limits for the global efficiency based on the 95% confidence in-

Table 3. Overall Collection Efficiencies and Pressure Drops

Design	ΔP (kPa)	η_m (%)	η_p (%) Sedigraph 5100D	η_p (%) Coulter LS230
RS_VHE	0.11	78.3 ± 4.2	[73.1, 84.9]	[79.6, 86.4]
Stairmand HE	0.09	57.2	[52.4, 63.5]	[62.1, 72.8]

$D = 0.02$ m; $Q = 2.5 \times 10^{-4}$ m^3/s.

terval for the mean value of Pe_p obtained from Eq. (1) as explained by Salcedo and Coelho (18). Thus, the Mothes and Löffler (5) model predicts well collection when the Sedigraph particle-size distribution is employed, but overpredicts collections made with the Coulter size distribution.

Grade Efficiencies

To obtain the grade efficiency curves, a series of runs were performed at flow rates varying from 2.5×10^{-4} to 4.2×10^{-4}m^3/s with the RS_VHE design and a single run with the Stairmand design at 2.5×10^{-4} m^3/s.

Sampling was performed isokinetically at the cyclone inlet and exit with a laser spectrometer (Grimm 1.108). This spectrometer counts particles larger than 0.3 μm, which are internally converted to a mass basis using a proprietary algorithm. Although the Grimm spectrometer has a built-in backfilter that may be used as a gravimetric check against the optical counting, it was impossible to handle this filter without appreciable losses. Also, the concentration measured from the Grimm dust monitor cannot be reliably used to obtain the global collection because an appreciable fraction of particles are less than 0.3 μm and cannot be counted. Thus, the mass concentrations obtained from the Grimm monitor will overpredict global collection (by as much as 10%) above the gravimetric data obtained.

The sampling velocity was measured at the sampling sites (centers) by hot bulb anemometry with a Testo 400 monitor. Because sampling at the cyclone inlet and outlet could not be simultaneously performed, several tests were carried out to establish a correct sampling time in which variations from the powder feeder and spectrometer were averaged. If sampling lasted for at least 30 minutes, then the average concentration was fairly constant (47). To test for errors due to gas swirling at the cyclone exit, we inserted a long 0.3-m straight tube downstream of the vortex exit, as suggested by Kessler and Leith (12). Because the dust concentrations with or without the straightening flow-tube extension were very similar, we concluded that for these small cyclones and particle sizes gas swirling does not affect sampling.

Figures 7 shows the grade efficiencies obtained and predictions based on the Mothes and Löffler (5) theory coupled with Eq. (1). The Mothes and Löffler model, in which the mean value of Pe_p obtained from Eq. (1) is used, overpredicts the grade efficiency curves. These results are in agreement with previously obtained data with small (0.043 and 0.023 m diameter) cyclones in which a similar test dust was used (see Figs. 4b and 4d in Salcedo and Coelho (18)). Also, the grade efficiency curve for the Stairmand HE design shows a shift toward larger particle sizes; this result agrees with the lower global collection obtained with this design compared to that found with the RS_VHE design. In addition, the Stairmand design shows signs of particle reentrainment for the larger sizes.

Figure 8 shows the grade efficiencies obtained with the RS_VHE cyclone at the maximum tested flow rate of 4.2×10^{-4} m^3/s. The Mothes and Löffler model (5) overpredicts collection, and no signs of particle reentrainment are evident at the larger diameters. The cyclone cut size decreased from approximately 0.8 μm at the lower flow rate to about 0.5 μm at the higher flow rate; the corresponding predicted values were 0.6 and 0.35μm, respectively. The Stairmand design shows a cut size of 2 μm at the lower flow rate. One-micrometer aerodynamic cut diameters at flow rates typical of industrial multicyclones (approximately 100–200 m^3/h) may be achieved under the Mothes and Löffler (5) model with the RS_VHE

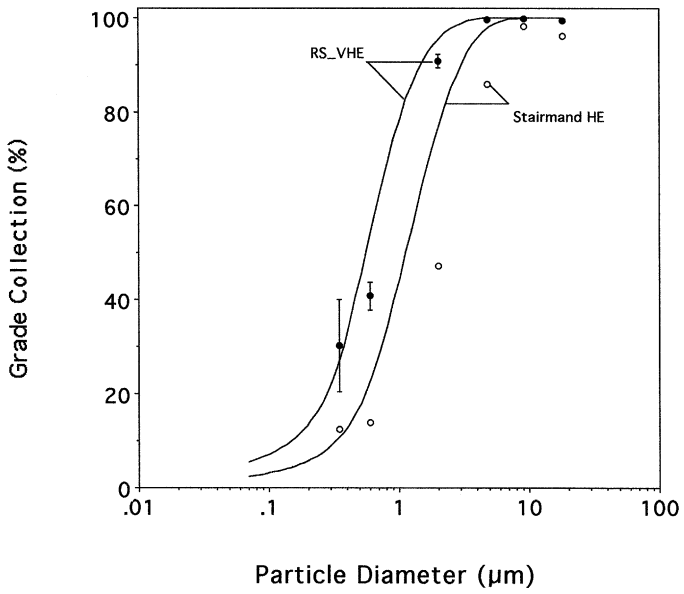

Figure 7. Predicted and measured grade efficiencies at 2.5×10^{-4} m^3/s.

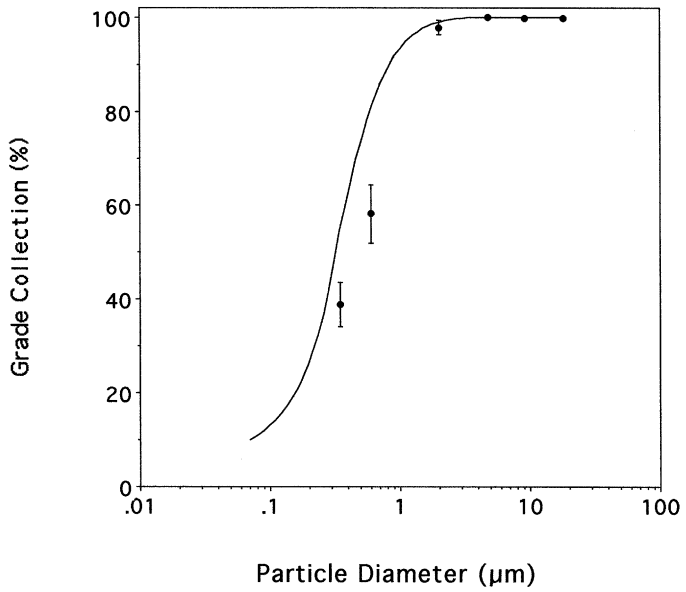

Figure 8. Predicted and measured grade efficiencies at 4.2×10^{-4} m^3/s.

design and 1.5-μm cut diameters can be achieved with the Stairmand or Swift HE designs at a pressure loss of 1.5 kPa.

Other Performance Indicators

At present, no dimensional number is known that would predict the cut size and the slope of the grade efficiency curve of a given cyclone with arbitrary geometry and for arbitrary operating conditions. However, cyclone manufacturers have long relied on a nondimensional number (Stokes's number) to represent cyclone performance. This number is usually given by (24,48)

$$\mathrm{Stk}_{50} = \frac{C_c d_{ae,50}^2 \rho_p u_{in}}{18 \mu D} \tag{11}$$

where C_c is the Cunningham correction factor and $d_{ae,50}$ is the aerodynamic cut size. This relation has been favored by designers because it gives an easy way to scale up cyclones on the basis of a single test curve (48). However, Stk_{50} (Stokes's number) depends not only on cyclone geometry but also on some pa-

rameter describing the gas flow, such as a Reynolds number; for example, as the Reynolds number increases, Stk_{50} decreases. Also, even for the same geometry and similar cyclone sizes and flow rates, considerable scatter is found in the available data (24). For comparison purposes, $(Stk_{50})^{1/2}$ was computed for both the Stairmand HE and RS_VHE designs with the experimental data given above. Svarovsky (48) and Lidén and Gudmundsson (24) provided information of this parameter from a number of sources and cyclone designs. For the Stairmand HE design, values of $(Stk_{50})^{1/2}$ ranged from 1.095×10^{-2} to 4.4×10^{-1}, depending on cyclone size and flow rate. Table 4 shows the computed value for this gas-flow parameter for the 2 test cyclones employed in the present work. The RS_VHE design showed a somewhat lower value, which decreased with an increase in flow rate, as expected.

Moore and McFarland (49,50) defined a cut-off size parameter as follows:

$$\Psi_{50} = \frac{\sqrt{C_c} d_{ae,50}}{D} \tag{12}$$

which is highly correlated with a Reynolds number based on the hydrodynamic cyclone body radius, calculated as

$$Re_{ann} = 0.5\left(1 - \frac{D_e}{D}\right)\frac{\rho u_{in} D}{\mu} \tag{13}$$

Lidén and Gudmundsson (24) showed for a series of 5 cyclone geometries (including the Stairmand HE design), with sizes ranging from 0.019 to 0.305 m, that Y_{50} is highly correlated with annular Reynolds Number (Re_{ann}). Also, the scatter was considerably reduced when the dependence of $(Stk_{50})^{1/2}$ values on the Reynolds number were compared. Figure 9 shows the range of experimental values computed by Lidén and Gudmundsson (24) for the 5 different cyclone geometries, excluding 2 data points that these authors considered to be outliers. The computed values of Ψ_{50} for the Stairmand HE employed in the present work (Table 4) is within the expected range, while the RS_VHE test cyclones showed somewhat lower (better) Ψ_{50} values.

Table 4. Cut-off $(Stk_{50})^{1/2}$ and Ψ_{50} Values (Dimensionless)

+ Design	$Q(m^3/s)$	$(Stk_{50})^{1/2}$	Ψ_{50}
RS_VHE	2.52×10^{-4}	0.013	6.42×10^{-5}
	4.20×10^{-4}	0.011	4.10×10^{-5}
Stairmand HE	2.52×10^{-4}	0.020	1.12×10^{-4}

Ψ_{50} is a dimensionless performance indicator.

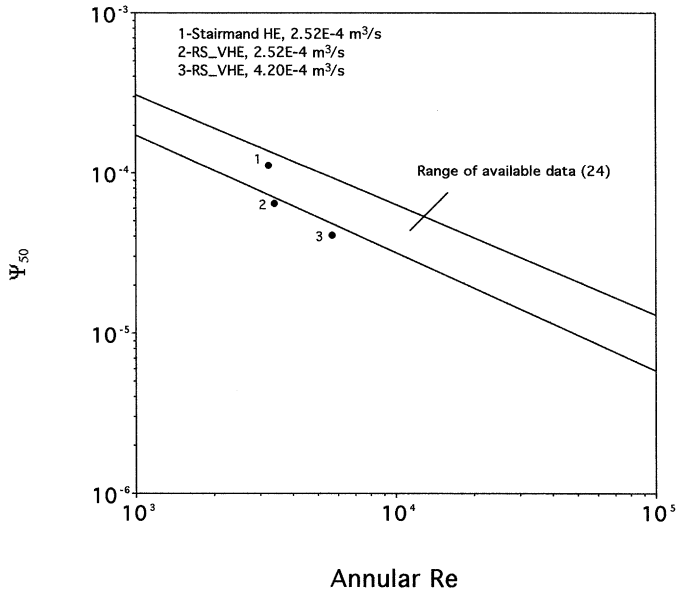

Figure 9. Experimental data on Ψ_{50} vs. Re_{ann} for the test cyclones and the experimental range from Lidén and Gudmundsson (24).

CONCLUSIONS

In this paper we have demonstrated that significantly improved reverse-flow cyclones can be designed through solved numerical optimization problems. These calculations maximize a profit function, such as global efficiency, that is subjected to the model equations (equality constraints) and inequality constraints (geometrical, pressure drop, and saltation velocity). The Mothes and Löffler (5) theory, coupled with an empirical estimate of the particle turbulent-dispersion coefficients, was used as a modeling environment, (18). We identified 2 different geometries, named RS_VHE and RS_K, that respectively maximize the global efficiency or the benefit-cost ratio proposed by Licht (28). Comparisons of the predicted performance of the highest-efficiency RS_VHE with other high-efficiency cyclones suggest the superiority of the proposed geometry. Laboratory-scale experiments with an optimized geometry for a small flow rate and fine particle size distribution at low loadings show the superiority of the proposed geometry over the Stairmand HE design or against a suboptimum design (34,40).

The decrease in emissions are expected to be above 30% with flow rates typical of industrial-scale multicyclones, when compared with those expected for the Stairmand or Swift HE designs. The proposed geometries have been granted a

Portuguese patent (PT B01D045/12) (51) and a European patent is being processing (38) for it.

Due to the very small scale of the tested cyclones, no warranty may be given to the performance of the optimized cyclones compared to other high-efficiency designs, either on a pilot or an industrial scale. To test the optimized cyclones at realistic scales, a cooperation program is underway between the Portuguese Innovation Agency, a large Portuguese chemical manufacturer, and the University of Porto to experimentally validate the expected increased performance of the proposed geometries in cyclones with diameters up to 0.46 m.

ACKNOWLEDGMENTS

The authors thank Fundação para a Ciência e a Tecnologia for financial support through contract PRAXIS/ P/EQU/12003/98.

NOMENCLATURE

s_Δ^2	sample variance between predicted and measured collection efficiency
a	height of tangential entry (m)
b	width of tangential entry (m)
C_c	Cunningham correction factor (dimensionless)
D	cyclone diameter (m)
$d_{ae,50}$	aerodynamic cyclone cut size (m)
D_b	cyclone dust discharge diameter (m)
D_e	vortex finder diameter (m)
d_p	Particle diameter (m)
D_r	dispersion coefficient (m^2/s)
h	height of cylindrical body (m)
H	total cyclone height (m)
I	mean sum of squares deviation between predicted and measured collection efficiencies
Pe_p	radial particle Peclet number
Q	volumetric flow rate ($N \cdot m^3/s$)
Re_p	radial particle Reynolds number
s	vortex finder length (m)
Stk_{50}	Stokes's number (Eq. 11, dimensionless)
T	absolute temperature (K)
u_{in}	mean entry velocity (m/s)
u_r	particle radial velocity (m/s)
u_s	saltation velocity (m/s)

Greek Letters

μ	gas viscosity (kg/m·s)
Δ	mean deviation between predicted and measured collection efficiency
ΔH	number of velocity heads (dimensionless)
ΔP	pressure loss (Pa)
ΔP_{max}	maximum allowable pressure drop (Pa)
Ψ_{50}	performance indicator (Eq. 12, dimensionless)
ε	semi-angle of cyclone cone (°)
η_m	measured collection efficiency
η_p	predicted collection efficiency
ρ	gas density (kg/m^3)
σ_g	geometric standard deviation (dimensionless)

REFERENCES

1. Lapple, C.E. Processes Use Many Collection Types. Chem. Eng. **1951,** *58* (5), 144–151.
2. Barth, W. Design and Layout of the Cyclone Separator on the Basis of New Investigations. BWK **1956,** *8* (*Heft 1*), 1–9.
3. Leith, D.; Licht, W. *The Collection Efficiency of Cyclone Type Particle Collectors—A New Theoretical Approach*; AIChE Symposium Series; 1972; Vol. 126, 196–206.
4. Dietz, P.W. Collection Efficiency of Cyclone Separators. AIChE J. **1981,** *27* (6), 888–892.
5. Mothes, H.; Löffler, F. Prediction of Particle Removal in Cyclone Separators. Int. Chem. Eng. **1988,** *28* (2), 231–240.
6. Li, E.; Wang, Y. A New Theory of Cyclone Separators. AIChE. J. **1989,** *35* (4), 666–669.
7. Iozia, D.L.; Leith, D. The Logistic Function and Cyclone Fractional Efficiency. Aerosol Sci. Techn. **1989,** *12,* 598–606.
8. Clift, R.; Ghadiri, M.; Hoffman, A.C. A Critique of Two Models for Cyclone Performance. AIChE J. **1991,** *37* (2), 285–289.
9. Bohnet, M.; Lorenz, T. Separation Efficiency and Pressure Drop of Cyclones at High Temperatures. In *Gas Cleaning at High Temperatures*; Clift, R., Seville, J.P.K., Eds.; Blackie Academic and Professional: Glasgow, UK; 1993; 17–31.
10. Salcedo, R.L.R. Collection Efficiencies and Particle Size Distributions from Sampling Cyclones—Comparison of Recent Theories with Experimental Data. Can. J. Chem. Eng. **1993,** *71* (1), 20–27.
11. Salcedo, R.L.; Fonseca, A.M. Grade-Efficiencies and Particle Size Distributions from Sampling Cyclones. In *Mixed-Flow Hydrodynamics;* Cheremisinoff, P., Ed.; Gulf Publishers: Houston, Texas; 1996; 539–561.

12. Kessler, M.; Leith, D. Flow Measurement and Efficiency Modeling of Cyclones for Particle Collection. Aerosol Sci. Technol. **1991,** *15,* 8–18.
13. Dirgo, J.; Leith, D. Cyclone Collection Efficiency: Comparison of Experimental Results with Theoretical Predictions. Aerosol Sci. Technol. **1985,** *4*, 401–415.
14. Hoffmann, A.C.; de Groot, M.; Hospers, A. The Effect of the Dust Collection System on the Flow Pattern and Separation Efficiency of a Gas Cyclone. Can. J. Chem. Eng. **1996,** *74* (4), 464–470.
15. Boysan, F.; Ayers, W.H.; Swithenbank, A. A Fundamental Mathematical Modelling Approach for Cyclone Design. Trans. Inst. Chem. Engrs. (London) **1982,** *60,* 222–230.
16. Heumann, W.L. Cyclone Separators: A Family Affair. Chem. Eng. **1991,** June, 118–123.
17. Ramachandran, G.; Leith, D. Cyclone Optimization Based on a New Empirical Model for Pressure Drop. Aerosol Sci. Technol. **1990,** *15,* 135–148.
18. Salcedo, R.L.; Coelho, M.A. Turbulent Dispersion Coefficients in Cyclone Flow—An Empirical Approach. Can. J. Chem. Eng. **1999,** *77* (4), 609–617.
19. Ogawa, A. Diffusion of the Fine Solid Particles in the Turbulent Rotational Air Flow in the Vortex Chamber. Bulletin of the JSME **1984,** *27* (226), 763–772.
20. Ogawa, A.. Diffusion of the Fine Solid Particles on the Concave Wall Surface in the Vortex Chamber. J. Coll. Engng. Nihon Univ. **1987,** *A-28* (March), 99–109.
21. Hoffmann, A.C.; van Santen, A.; Allen, R.W.K. Effects of Geometry and Solid Loading on the Performance of Gas Cyclones. Powder Technol. **1992,** *70,* 83–91.
22. Li, Z.; Zisheng, Z.; Kuotsung, Y. Study of Structure Parameters of Cyclones. Chem. Eng. Res. Des. **1988,** *66,* 114–120.
23. Schmidt, P. Unconventional Cyclone Separators. Int. Chem. Eng. **1993,** *33* (1), 8–17.
24. Lidén, G.; Gudmundsson, A. Semi-empirical Modelling to Generalise the Dependence of Cyclone Collection Efficiency on Operating Conditions and Cyclone Design. J. Aerosol Sci. **1997,** *28* (5), 853–874.
25. Dirgo, J.; Leith, D. Performance of Theoretically Optimized Cyclones. Filt. Sep. **1985,** *22* (March/April), 119–125.
26. Iozia, D.L.; Leith, D. Cyclone Optimization. Filt. Sep. **1989,** 272–274.
27. Dirgo, J. Relationships Between Cyclone Dimensions and Performance. Ph.D. diss., Harvard University, Cambridge, Mass, 1988.
28. Licht, W. *Air Pollution Control Engineering—Basic Calculations For Particulate Collection;* Marcel Dekker: New York and Basel, Switzerland, 1980; 233–264.
29. Cooper, D.W. Cyclone Design: Sensitivity, Elasticity, and Error Analysis. Atmos. Environ. **1983,** *17,* 485.

30. Coker, A.K. Understand Cyclone Design. Chem. Eng. Progress **1993,** 51–55.
31. Shepherd, C.B.; Lapple, C.E. Flow Pattern and Pressure Drop in Cyclone Dust Collectors. Ind. Eng. Chem. **1939,** *31,* 979.
32. Caplan, K.J. Source Control by Centrifugal Source and Gravity. In *Air Pollution;* Stern, A.C., Ed.; Academic Press: New York, 1968; Vol. 43, 366–377.
33. Alexander, R.M. Fundamentals of Cyclone Design and Operation. Proc. Aus. Inst. Min. Met. NS **1949,** *152* (3), 152–153, 203–228.
34. Campos, J.A.G. Optimized Design of Reverse-Flow Cyclones: A New Approach. M.Eng. Thesis, Faculdade de Engenharia da Universidade do Porto, Porto Codex, 1998. (in Portuguese)
35. Salcedo, R.; Gonçalves, M.J.; Feyo de Azevedo, S. An Improved Random-Search Algorithm for Non-linear Optimization. Comp. and Chem. Engng. **1990,** *14* (10), 1111–1126.
36. Salcedo, R.L. Solving Nonconvex NLP and MINLP Problems with Adaptive Random-Search. Ind. Eng. Chem. Res. **1992,** *31* (1), 262–273.
37. Cardoso, M.F.; Salcedo, R.L.; Feyo de Azevedo, S.; Barbosa, D. Optimization of Reactive Distillation Processes with Simulated Annealing. Chem. Eng. Sci. **2000,** *55* (21), 5059–5078.
38. Salcedo, R.L.R. High Efficiency Cyclones, EP0972572A2, European Patent Application 99670006.8, Bulletin 2000103, January 19, 2000.
39. Ogawa, A. *Separation of Particles from Air and Gases;* Beddow, J.K., Ed.; CRC Press: Boca Raton, Fla, 1984; Vol. II, 15–16.
40. Salcedo, R.L.; Campos, J.A.G. In *Optimization for Pollution Reduction: A Numerical Approach to Cyclone Design*, 2nd Conference on Process Integration, Modeling and Optimization for Energy Saving and Pollution Reduction, Budapest, Hungary, May 31–June 2, 1999; Friedler, F. (Univ. of Veszprém) and Rlemes, J. (UMIST); 571–576.
41. Wright, B.M. A New Dust Feed Mechanism. J. Sci. Instrum. **1950,** *27,* 12–15.
42. Bott, S.E.; Hart, W.H. Extremely Wide Dynamic Range, High-Resolution Particle Sizing by Light Scattering. In *Particle Size Distribution II: Assessment and Characterization*; Provder, Ed.; ACS Symposium Series; 1991; Vol. 472.
43. Diamond, S. Rapid Particle Size Analysis of Fly Ash with a Commercial Laser Diffraction Instrument. Mat. Res. Soc. Symp. Proc. **1988,** *113,* 119–127.
44. Fonseca, A.M.; Órfão, J.J.; Salcedo, R.L. Kinetic Modeling of the Reaction of HCl and Solid Lime at Low Temperatures. Ind Eng. Chem. Res. **1999,** *37* (12), 4570–4576.
45. Allen, T. *Particle Size Measurement.* Chapman and Hall, Ltd: London, 1968.

46. Barreiros, F.M.; Ferreira, P.J.; Figueiredo, M.M. Calculating Shape Factors from Particle Sizing Data. Part. Part. Syst. Charact. **1996,** *13,* 368–373.
47. Cândido, M.G. Recirculation Cyclones for Fine Particle Collection. M.Eng. thesis, University of Porto, Porto Codex, 2000. (in Portuguese)
48. Svarovsky, L. Solid-Gas separation. Elsevier Scientific Publishing, New York, **1981,** 33–52.
49. Moore, M.E.; McFarland. Performance Modeling of Single-Inlet Aerosol Sampling Cyclones. Environ. Sci. Technol. **1993,** *27,* 1842–1848.
50. Moore, M.E.; McFarland, A.R. Design Methodology For Multiple-Inlet Air Sampling Cyclones. Environ. Sci. Technol. **1996,** *30,* 271–276.
51. Salcedo, R.L.R. Ciclones de Elevada Eficiência, PT 102166, Instituto National de Propriedade Industrial, December 22, 1999.

Received June 2000
Revised November 2000